Available online at www.sciencedirect.com

SciVerse ScienceDirect

Journal of the European Ceramic Society 32 (2012) 795–805

www.elsevier.com/locate/jeurceramsoc

Onset coarsening–coalescence kinetics of ZrO_2 and less refractory TiO_2 nanoparticles: Effect of homologous temperature and phase transformation

Tzu-Jung Chen, Jer-Han Lu, Hui-Di Lu, I-Lung Liu, Pouyan Shen *

Department of Materials and Optoelectronic Science, National Sun Yat-sen University, Kaohsiung 80424, Taiwan, ROC

Received 17 August 2011; accepted 17 October 2011
Available online 15 November 2011

Abstract

Specific surface area change of ZrO_2 (predominant tetragonal – (t) symmetry, 30–50 nm) and less refractory TiO_2 anatase nanoparticles (20–50 nm) upon isothermal firing at 700–1000 °C in air was determined by N_2 adsorption–desorption hysteresis isotherm. The nanoparticles underwent onset coarsening–coalescence within minutes without appreciable phase transformation for TiO_2, but with extensive transformation into monoclinic (m-) symmetry for ZrO_2. The apparent activation energy of such a process being not much higher for ZrO_2 (77 ± 23 kJ/mol) than TiO_2 (56 ± 3 kJ/mol) nanoparticles can be attributed to transformation plasticity. The minimum temperature for coarsening/coalescence of the present ZrO_2 and TiO_2 nanoparticles was estimated as 710 and 641 °C, respectively.
© 2011 Elsevier Ltd. All rights reserved.

Keywords: Onset coarsening–coalescence; ZrO_2; TiO_2; Nanoparticles; BET; BJH

1. Introduction

Zirconium and titanium dioxides are important ceramic materials for many engineering applications. Zirconia (ZrO_2) was widely used as thermal sensor,[1] whereas tetragonal (t-) zirconia polycrystals (TZP) have a beneficial transformation toughening effect of martensitic t- to monoclinic (m-) transformation under stress[2,3] and even fair ductility at low temperatures when the crystal size falls in nanometers.[4] As for anatase TiO_2, it has important optocatalytic applications[5] and is thermodynamically more stable than rutile when the particle size is below ~14.5 nm.[6,7] The surface area reduction and durability of nanosized particles in a specific temperature range are of concern to the preparation and heterogeneous catalysis use[8] of the two oxides in thin film[9,10] or bulk assembly upon thermal exposure in a static or dynamic process. It is thus of great interest to clarify whether vigorous onset coarsening–coalescence events of the tetragonal (t-) ZrO_2 and anatase-type TiO_2 nanoparticles proceed before their transformation into the stable polymorphs.

From thermodynamic viewpoint, nanosized particles having relatively high specific surface area and low melting point[11] and hence a beneficial high homologous temperature (T/T_m, where T_m is melting point in Kelvin) than the bulk are expected to coarsen, coalesce and/or sinter rapidly at relatively low temperatures. This has been recently proved for close-packed oxide nanoparticles with varied shape, i.e. equiaxed γ-Al_2O_3,[12] platy cobalt oxide[13] and hexagonal rod of ZnO[14] based on electron microscopic observations coupled with BET/BJH measurements of specific surface area and pore size/shape change of the dry-pressed samples subjected to isothermal firing at temperatures for minutes. (BET and BJH denote Brunauer–Emmett–Teller method[15] and Barrett–Joyner–Halenda method,[16] respectively.) The specific-surface-area change rate in the steady state was used to determine the apparent activation energy of a vigorous onset coarsening–coalescence event for these oxide nanoparticles.[12–14] In addition, the minimum temperature for $\{0\ 1\ \bar{1}\ 0\}$- and $(0\,0\,0\,1)$-specific coarsening/coalescence of the hexagonal ZnO nanorods was estimated to be 516 °C based on the extrapolation of steady specific surface area reduction rates to null.[14]

Here the BET/BJH method is further employed to compare the onset coarsening–coalescence kinetics of nanosized ZrO_2 ($T_m = 3023$ K) and much less refractory TiO_2 ($T_m = 2116$ K) with bulk melting temperatures noted in parenthesis. We focused on the activation energy and minimum temperatures for incipient

* Corresponding author.
E-mail address: pshen@mail.nsysu.edu.tw (P. Shen).

0955-2219/$ – see front matter © 2011 Elsevier Ltd. All rights reserved.
doi:10.1016/j.jeurceramsoc.2011.10.023

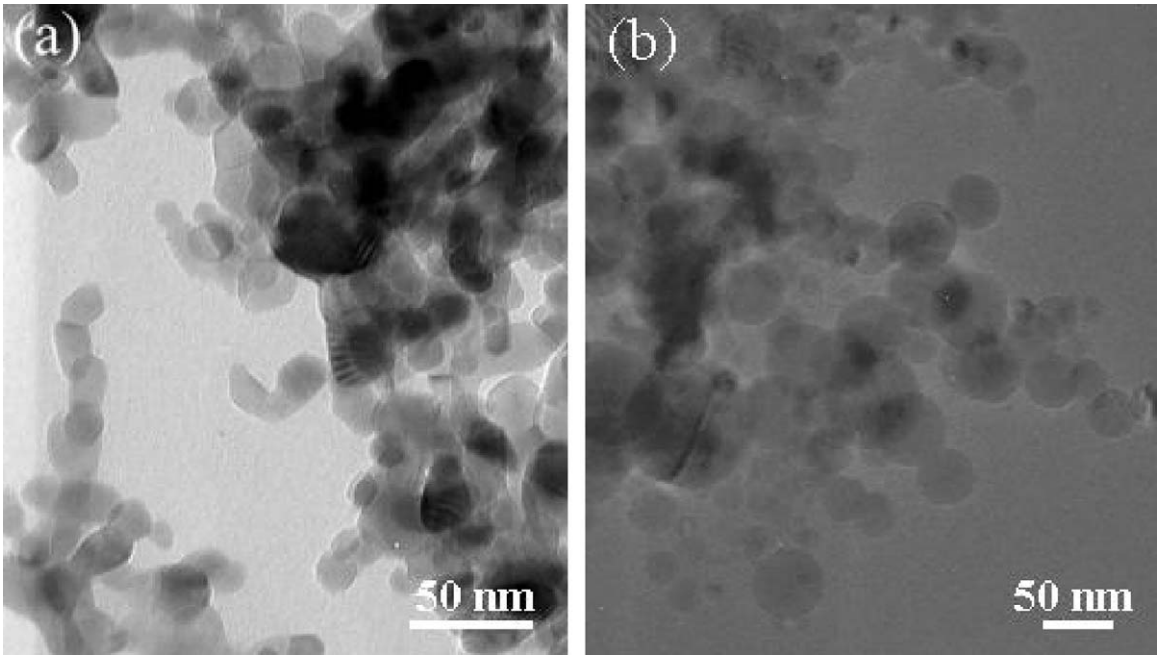

Fig. 1. TEM bright field image of the slightly faceted powders: (a) ZrO_2 and (b) TiO_2 having 20–50 nm and 30–50 nm in size, respectively. The TiO_2 particles are occasionally up to 100 nm in diameter.

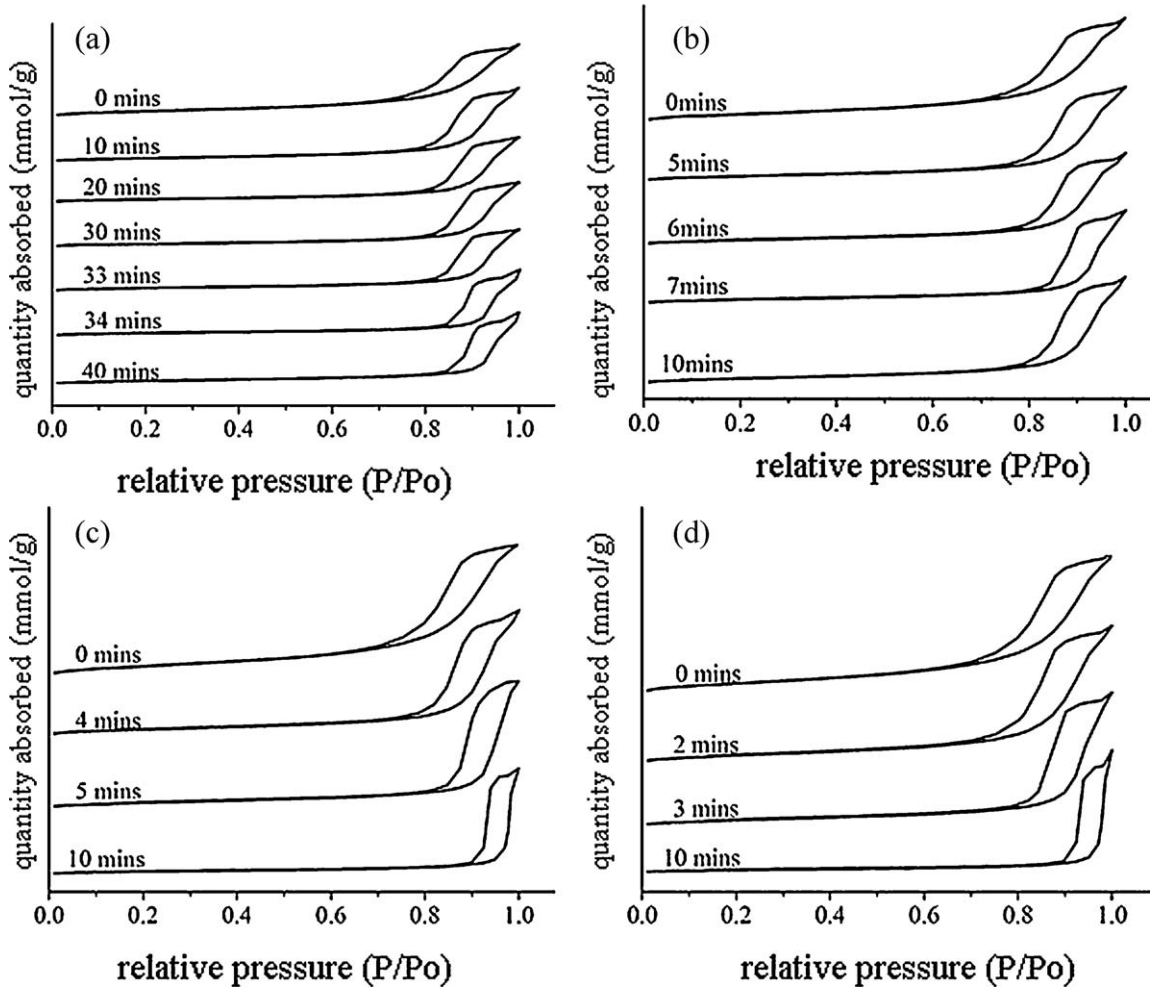

Fig. 2. BJH N_2 adsorption–desorption hysteresis isotherms of the ZrO_2 powder with an average size of <50 nm and subjected to the specified heating treatments: (a) 700 °C, 0–40 min, (b) 800 °C, 0–10 min, (c) 900 °C, 0–10 min, and (d) 1000 °C, 0–10 min.

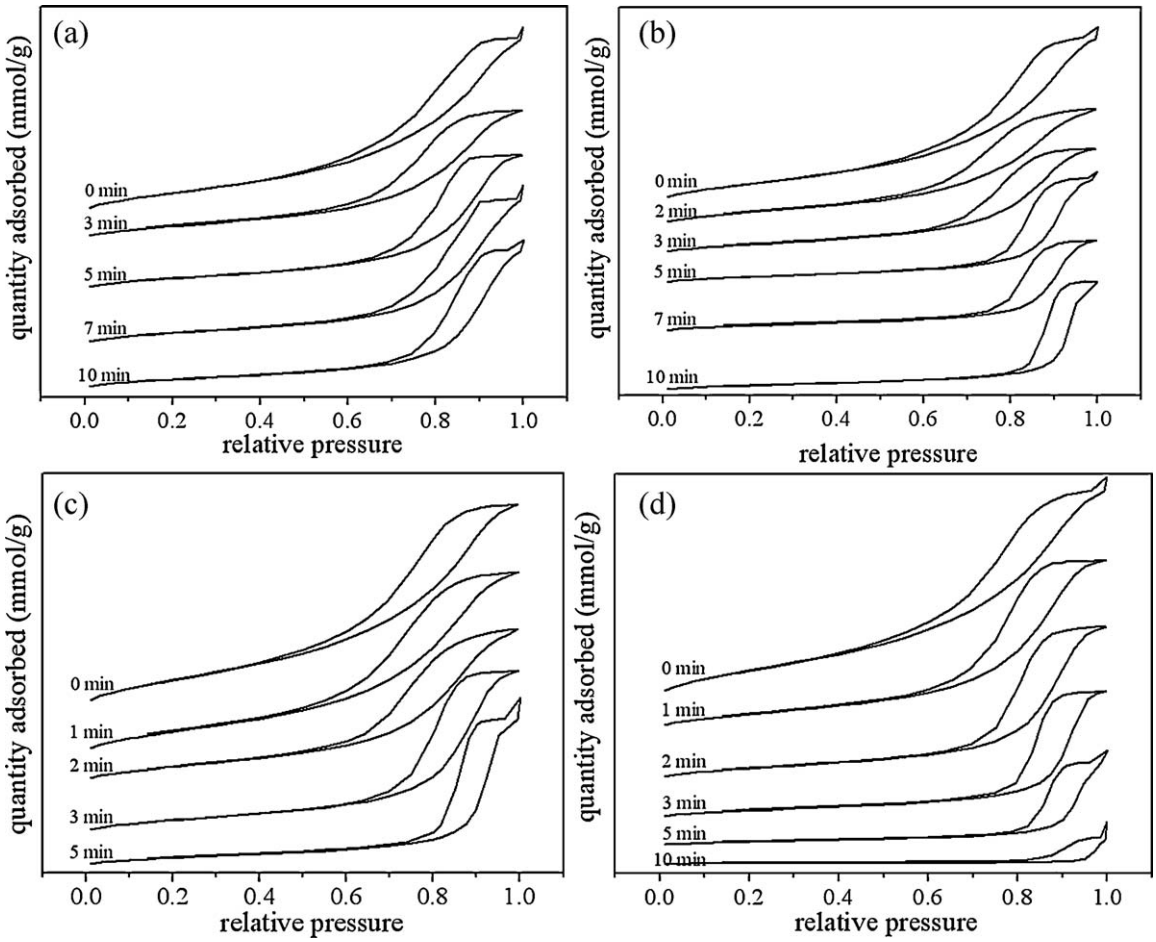

Fig. 3. BJH N_2 adsorption–desorption hysteresis isotherms of the TiO_2 powder with an average size of <50 nm and subjected to the specified heating treatments: (a) 700 °C, 0–10 min, (b) 800 °C, 0–10 min, (c) 900 °C, 0–5 min, and (d) 1000 °C, 0–10 min.

coarsening–coalescence of the nanoparticles and the underlying effect, if any, of the polymorphic transformation below a critical specific surface area. This subject is not only of interest to ZrO_2 sensor[1] and TiO_2 photocatalytic applications at temperatures[5] but also accounts for rapid assembly of nanocondensates by flame reactors, gas evaporation method[17] or pulsed laser ablation (PLA) under the influence of radiant heating.[18–21]

2. Experimental

ZrO_2 (Aldrich, 99.7% with t- and minor m-phase) and TiO_2 anatase (Aldrich, 99.7%) powders predominantly less than 50 nm in size were die-pressed at 650 MPa into disks ca. 5 mm in diameter and 2 mm in thickness followed by isothermal firing at 700–1000 °C corresponding to homologous temperature (T/T_m in Kelvin) range 0.32–0.42 and 0.46–0.60, respectively in air. The disks were fired in 5–10 min increments at 700 and 800 °C and 1–2 min increments at 900 and 1000 °C in air, until onset coarsening–coalescence was noted by the type of adsorption–desorption hysteresis isotherm. The starting powders were dispersed on a carbon-coated collodion film for phase, shape and size distribution characterizations using transmission electron microscopy (TEM, JEOL 3010 at 300 kV). Microstructure changes of the samples due to dry pressing and heating were studied by scanning electron microscopy (SEM, JEOL 6330 at 10 kV). The phase identity of the dry pressed and heat treated samples was determined mainly by X-ray diffraction (XRD, CuKα, 40 kV, 30 mA at 0.05° and 3 s per step).

Nitrogen adsorption/desorption isotherms of the dry pressed and then heated powders were conducted at liquid nitrogen temperature of 77 K using a Micromeritics ASAP 2020 instrument. The surface area and pore size distributions were obtained from the N_2 adsorption and desorption branch, using the BET[15] and BJH method,[16] in low and high relative pressure (P/P_0) range, respectively where P_0 is the saturation pressure determined as 760–762 mmHg. A filler rod containing ca. 0.1 g of ZrO_2 and 0.7 g of TiO_2 sample with a theoretical density of 5.9 g/cm^3 (assuming a negligible difference from that of the parent fluorite type) and 3.9 g/cm^3, respectively was pumped down to 10^{-3} Torr for degassing at 300 °C followed by BET/BJH measurements at a relative pressure increment 0.05. The BET isotherm and BJH adsorption/desorption hysteresis type of the samples are classified according to the scheme of International Union of Pure and Applied Chemistry (IUPAC).[22] The H1 type adsorption/desorption hysteresis loop of the type IV isotherm (cf. Appendix 1 of Ref. 12) was used as an indicator of cylindrical pore formation and onset coarsening–coalescence or possible sintering.

Table 1
BET/BJH data and phase identity of ZrO_2 powder subjected to various treatments.

T (°C)-t (min)	Specific surface area (m^2/g)	Ads./desorp. pore width (nm)	Phases
Dry pressed	38.05 (S_0)	12.9/11.5	t > m
700-10	27.85	20.0/15.0	t + m
700-20	23.48	19.8/14.7	t + m
700-30	21.30	20.6/14.9	m > t
700-35	20.75	24.2/18.0	m ≫ t
700-40	21.11	21.4/17.7	m
700-50	18.43	24.9/17.7	m
800-5	26.45	19.2/13.8	t + m
800-6	25.29	19.0/14.5	t + m
800-7	20.54	21.8/15.9	m > t
800-8	23.25	21.6/16.0	m ≫ t
800-10	16.94	29.2/17.5	m
800-20	13.58	39.5/21.8	m
800-30	15.64	30.6/20.1	m
800-40	12.86	36.3/20.0	m
800-50	13.20	34.1/20.7	m
900-4	22.07	18.8/14.1	t + m
900-5	19.60	25.1/18.6	m > t
900-6	16.99	25.0/16.4	m ≫ t
900-10	10.62	45.3/25.2	m
900-20	10.16	39.5/25.9	m
900-30	11.39	26.7/23.7	m
900-40	9.64	38.8/26.5	m
900-50	9.23	52.2/30.2	m
900-60	9.31	48.1/29.6	m
1000-2	28.32	16.7/12.9	t + m
1000-3	21.09	22.8/16.3	m > t
1000-5	13.51	33.9/20.5	m ≫ t
1000-10	8.67	56.5/30.7	m
1000-20	7.56	40.9/29.9	m
1000-30	7.82	42.0/32.6	m
1000-40	8.23	29.3/27.1	m
1000-50	7.21	33.7/28.3	m
1000-60	6.88	44.7/33.6	m

Note: Ads./desorp. denotes adsorption/desorption. The identity of phases is based on XRD and S_0 is the average of 4 independent observations.

3. Results

3.1. Size, shape and phase identity of nanoparticles

TEM observations by bright field image indicated that the starting ZrO_2 powders are equi-axed with slight facets and ca. 30–50 nm in diameter (Fig. 1a). The twinned m-ZrO_2 nanoparticles are due to polymorphic transformation from the predominant t-phase. The TiO_2 powders are also equi-axed with a predominant size of 20–50 nm although minor abnormal large particles up to 100 nm in size were occasionally observed (Fig. 1b). Regardless of the size difference, the TiO_2 powders remained as anatase with slight facets.

XRD (Appendix 1) confirmed that the starting ZrO_2 powders have a predominant t-phase and minor m-phase. However, t → m transformation occurred for the ZrO_2 powders upon isothermal dwelling in the temperature range of 700–1000 °C because m-phase is stabilized below ca. 1200 °C under ambient pressure condition.[23] As for the TiO_2 powders, the anatase → rutile transformation did not occur except fired for a long time at a relatively high temperature, e.g. more than 7 min at 1000 °C.

3.2. BET/BJH observations of pore and specific surface area changes by firing

BET data of the fired samples indicated that the specific surface area decreases whereas average pore size increases with the increase of dwelling time at a specific firing temperature for ZrO_2 and TiO_2 powders as compiled in Tables 1 and 2, respectively. The drastic change of specific surface area and average pore size are related to the formation of cylindrical and/or truncated pores as further revealed by the following BJH analyses.

The BJH N_2 adsorption–desorption hysteresis isotherms of the ZrO_2 powders dry pressed and further fired at 700, 800, 900 and 1000 °C for specified time periods (Fig. 2a, b, c and d, respectively) show hysteresis loops in the relative pressure range 0.75–1.0 (i.e. actual pressure range 571.5–762 mmHg). The dry pressed sample has H2 and H1 mixed type loop. The time to form nearly perfect H1 type loop, as an indicator of cylindrical pore formation and specific surface area reduction rate, decreases with the increase of firing temperature. The time of specific surface area reduction by ~50% with respect to the dry pressed sample are 39 ± 10, 8 ± 3, 5 ± 0.7 and 4 ± 0.3 min at 700, 800,

Table 2
BET/BJH data and phase identity of TiO_2 powder subjected to various treatments.

T (°C)-t (min)	Specific surface area (m^2/g)	Ads./desorp. pore width (nm)	Phases
Dry pressed	150.55 (S_0)	7.3/6.5	Anatase
700-3	110.08	8.7/7.6	Anatase
700-5	85.61	10.7/9.1	Anatase
700-7	85.45	11.6/10.1	Anatase
700-8	88.10	12.2/10.0	Anatase
700-10	70.89	13.5/11.4	Anatase
800-2	110.21	8.0/7.0	Anatase
800-3	83.83	9.5/8.2	Anatase
800-4	81.06	11.6/9.6	Anatase
800-5	55.71	14.5/11.9	Anatase
800-7	50.05	14.6/11.7	Anatase
800-10	44.71	19.7/16.2	Anatase
800-60	37.28	21.9/18.1	Anatase
900-1	116.25	7.4/6.5	Anatase
900-2	81.70	8.7/7.4	Anatase
900-3	66.94	11.4/9.5	Anatase
900-4	49.64	17.1/13.3	Anatase
900-5	40.79	17.5/13.6	Anatase
1000-1	85.28	9.4/8.0	Anatase
1000-2	60.45	14.1/11.0	Anatase
1000-3	41.25	15.4/12.2	Anatase
1000-5	22.25	19.0/14.5	Anatase
1000-10	3.92	43.9/28.2	Rutile
1000-60	4.19	32.5/19.8	Rutile

900 and 1000 °C, respectively (Table 1, cf. rate curves in Fig. 6). A longer firing time up to 60 min in this temperature range did not change much the H1 type loop indicating cylindrical pores are still dominating in such fired samples.

The adsorption–desorption hysteresis isotherms are quite different for the samples made of TiO_2 powders as compiled in Fig. 3. The green body consisting of such powders shows H2 type loop in a wider relative pressure range (0.5–1.0) than ZrO_2 presumably due to different surface state of the TiO_2 and ZrO_2 powders besides a wider size distribution of the latter. The loop shifts to a higher relative pressure and changes into H1 type, corresponding to cylindrical pore formation of the samples fired for ca. 10 min at 700 °C (Fig. 3a), 5 min at 800 °C (Fig. 3b), 3 min at 900 °C (Fig. 3c) and 1000 °C (Fig. 3d). Considering further the specific surface area change relative to the dry pressed sample (Table 2), the onset time for a total of 50% drop of the specific surface area and accompanied cylindrical pore formation was determined as 8 ± 2, 4 ± 0.9, 3 ± 0.5, and 1 ± 0.09 min for 700, 800, 900 and 1000 °C, respectively. A longer firing time in this temperature range improves the H1 type loop and shifts it toward a higher relative pressure (0.7–1.0), presumably due to repacking of the nano-sized powders as discussed later. A firing time of 10 min at 1000 °C was enough to cause the change of H1 type loop into irregular shape (Fig. 3d) due to the formation of the truncated pores from cylindrical ones.

3.3. SEM observations of microstructures

In general, dry pressing did not cause appreciable cracking and particle size change but cause significant agglomeration for the finer sized particles as indicated by SEM secondary electron

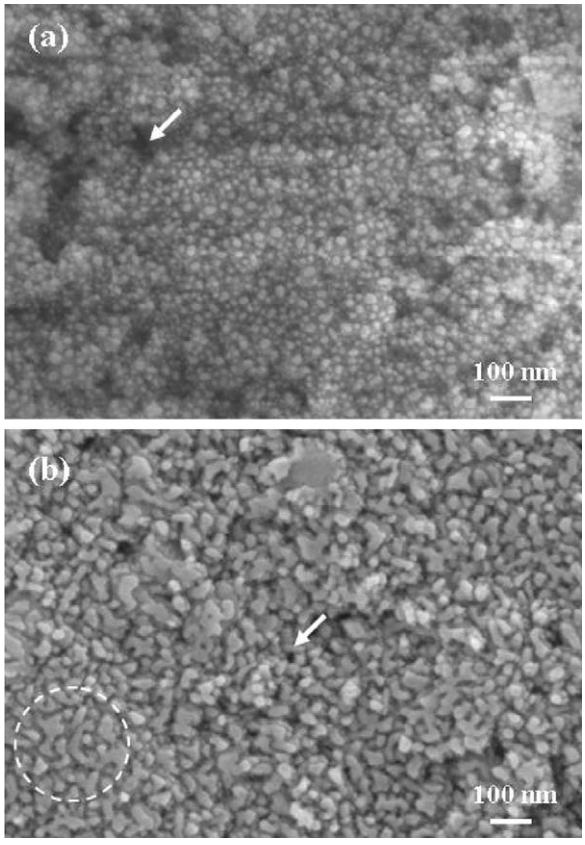

Fig. 4. SEM secondary electron image of the ZrO_2 powder: (a) dry pressed and slightly agglomerated with pores (arrow), and (b) further heated at 900 °C for 5 min to form cylindrical pores (arrow) and to slightly coarsen and repack the particles (circle).

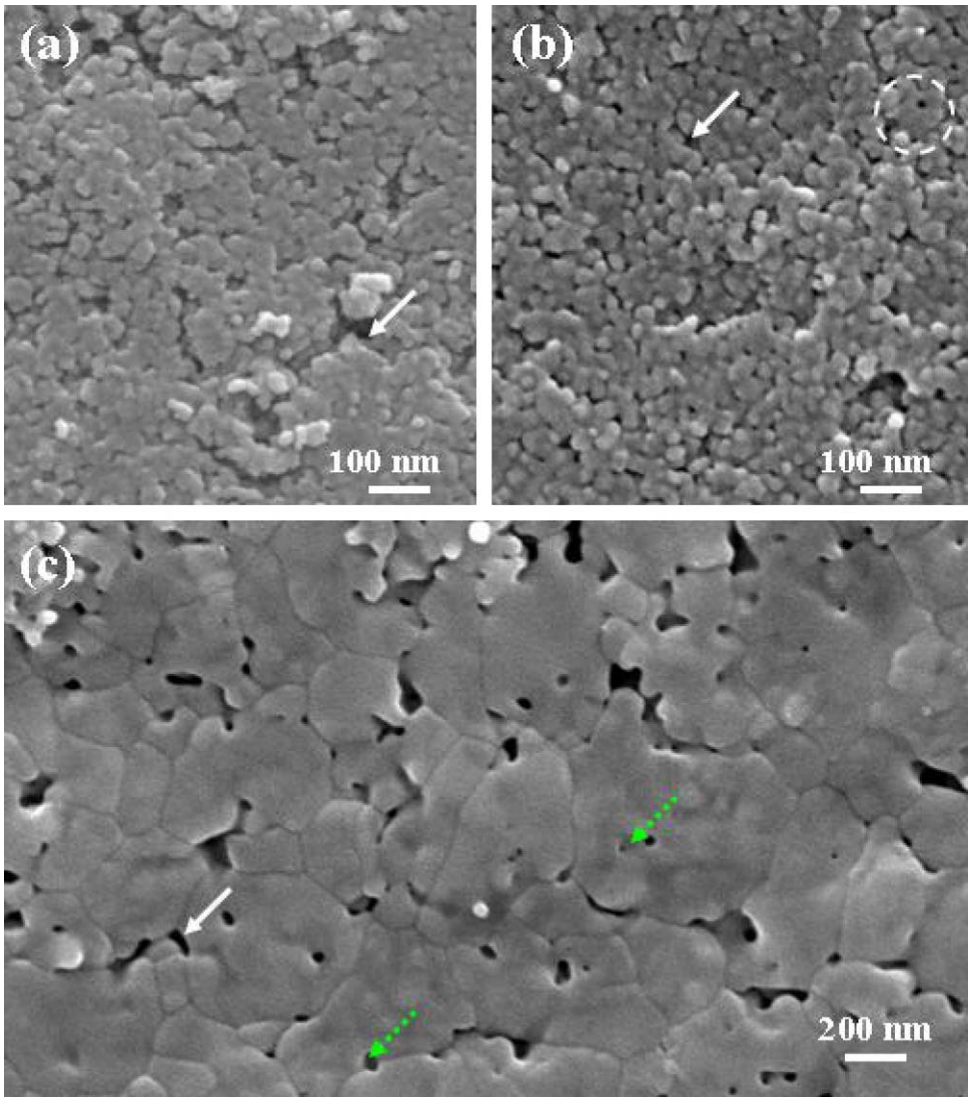

Fig. 5. SEM secondary electron image of the TiO_2 powder: (a) dry pressed and slightly agglomerated, and (b) further heated at 800 °C for 7 min to form cylindrical pores at grain junctions (white arrow) and among repacked anatase nanoparticles (circle) and (c) further heated at 1000 °C for 10 min to show cylindrical pores (white arrow) and truncated intra- and intergranular pores (green dashed arrow). (For interpretation of the references to color in this figure legend, the reader is referred to the web version of the article.)

images of the two samples with different average particle size in Figs. 4a and 5a. In both cases, the cylindrical pores characteristic of slightly sintered bodies are vague, and the relative density is difficult, if not impossible, to measure because the dry pressed powders tended to disperse in water during such measurements.

The occurrence of cylindrical pores, an indicator of onset coarsening/coalescence, in the samples fired for a suitable time period at a specified temperature was confirmed by SEM observations, as shown representatively in Figs. 4b and 5b, for TiO_2 and ZrO_2, respectively. Significant repacking and coalescence of slightly coarsened particles to form irregular shaped islands was observed to be associated with the sintering process in particular for the ZrO_2 particles (Fig. 4b). The truncated pores, an indicator of further coarsening/coalescence or even sintering, were observed only for the TiO_2 sample when fired at 1000 °C for 10 min for significant coarsening (Fig. 5c) accompanied with anatase → rutile transformation as mentioned.

4. Discussion

4.1. Adsorption–desorption hysteresis loop characteristic of mesopore change

Capillary condensation typically occurs for mesopores in a size range 2–50 nm to show type IV isotherm, which can be classified into H1 to H4 subtypes[22] (cf. Appendix 1 in Ref. 12). According to the present observations of BJH N_2 adsorption–desorption isotherms, the dry pressed TiO_2 and ZrO_2 powders have a hysteresis loop somewhat between H1 and H2 type.

Regardless of the difference in powder size, the TiO_2 and ZrO_2 samples just went through an onset coarsening–coalescence event have cylindrical mesopores with a characteristic H1 type hysteresis loop similar to the case of other mesoporous materials with a pore width range 2–50 nm.[22]

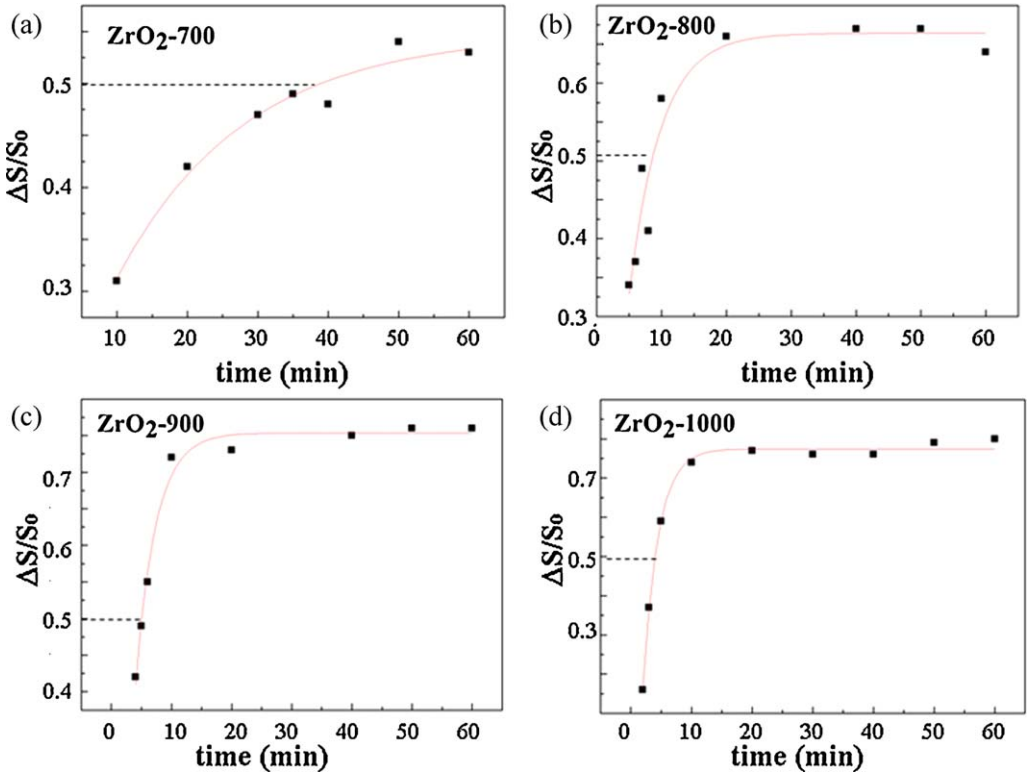

Fig. 6. Observed rate curves in terms of percent reduction of specific surface area ($\Delta S/S_0$, where S_0 is the initial quantity) versus time for nanosized ZrO_2 powders at specified temperatures from 700 to 1000 °C. The time $t_{0.5}$, i.e. with 50% reduction of specific surface area as denoted by dashed line, used for activation energy estimation, falls within an almost linear region.

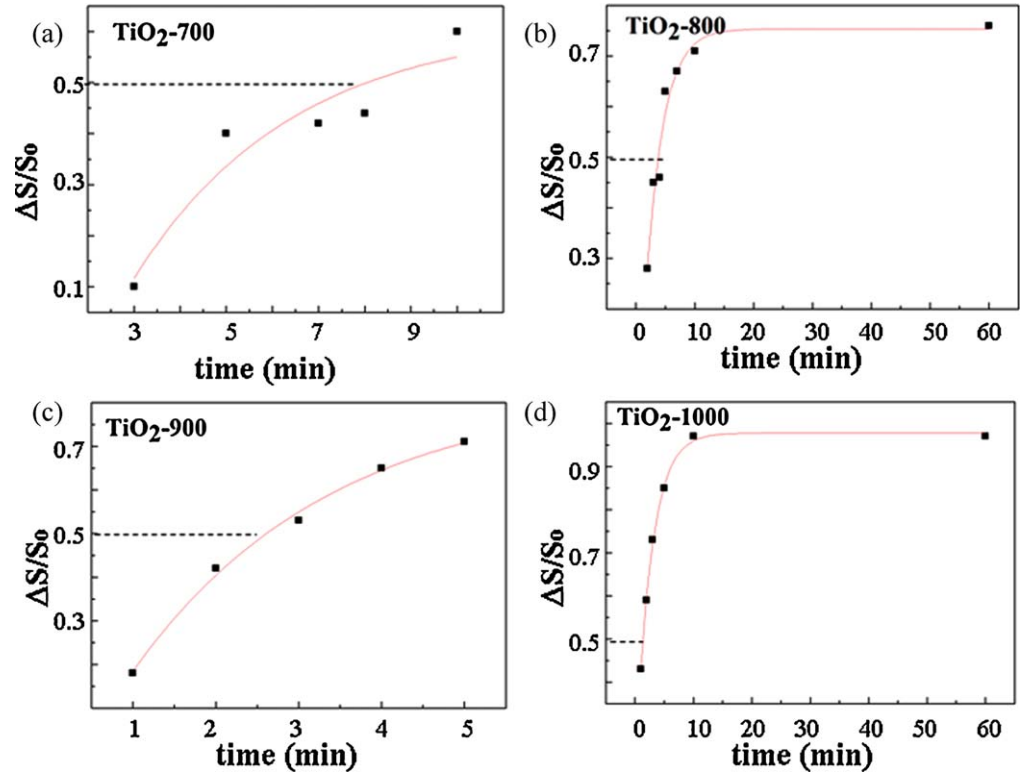

Fig. 7. Observed rate curves in terms of per cent reduction of specific surface area ($\Delta S/S_0$, where S_0 is the initial quantity) versus time for nanosized TiO_2 powders at specified temperatures from 700 to 1000 °C. The time $t_{0.5}$, i.e. with 50% reduction of specific surface area as denoted by dashed line, used for Activation energy estimation, falls within an almost linear region.

The kinetics to form cylindrical mesopores, however, depends on the size and shape of the starting powders. In general, the faceted and more uniform-sized ZrO_2 powders (30–50 nm) have a considerable larger pore size than the spherical TiO_2 powders with a wider distribution of particle size (20–50 nm) given the same firing temperature and time (Tables 1 and 2). Having a smaller pore size, the TiO_2 samples would allow easier pore migration and growth/coalescence at temperatures. This accounts for a wider size distribution of pores and less well-defined H1 type loop in a wider range of relative pressure for the TiO_2 powders upon firing. A longer firing time in the temperature range 700–1000 °C improved the H1 type loop for both ZrO_2 and TiO_2 powders due to a pronounced coarsening and repacking process of nanoparticles for effective sintering,[24] as the case of γ-Al_2O_3 nanoparticles.[12] On the other hand, the pores among the coarsened and repacked TiO_2 particles drastically doubled in size when the fire time increased from 5 to 10 min at 1000 °C (Table 2) corresponding to the necking of the cylindrical pores to form truncated pores and the anatase → rutile transformation accompanied with a significant density increase from 3.82–3.97 to 4.23–5.5.[25] In any case, surface energy change as the combined results of size, shape and phase identity of the nanoparticles would also affect the kinetics of N_2 adsorption and desorption and hence the hysteresis loop.

4.2. *Thermally activated coarsening–coalescence of nanoparticles under additional influence of phase transformation*

The present experimental results indicated that ZrO_2 and anatase TiO_2 nanoparticles were thermally activated at homologous temperature range 0.32–0.42 and 0.46–0.60 (based on bulk T_m 3023 K and 2116 K, respectively) in air for a vigorous coarsening–coalescence event. In addition, our previous study indicated that γ-Al_2O_3 nanoparticles were thermally activated at 1100–1400 °C, i.e. homologous temperature range 0.59–0.72 based on bulk T_m 2311 K, in air for the same event. The supposedly more refractory ZrO_2 turned out to be activated at much lower homologous temperature than TiO_2 and Al_2O_3. The apparent activation energy is essential to address this point as following.

On the basis of the drastic decrease of specific surface area by 50% (Tables 1 and 2) in the linear region of the rate curves (Figs. 6 and 7), the onset time $t_{0.5}$ for ZrO_2 and TiO_2 powders to coarsen and coalesce were determined, respectively. The onset time $t_{0.5}$ for ZrO_2 with accompanied t → m transformation (Table 1) turned out to be 39 ± 10, 8 ± 3, 5 ± 0.7, and 4 ± 0.3 min at 800, 900, 1000 and 1100 °C, respectively. The corresponding Arrhenius plot of the reciprocal time $t_{0.5}$ for onset coarsening–coalescence versus the reciprocal temperature in Kelvin gives an apparent activation energy 77 ± 2 kJ/mol considering the maximum uncertainty of each data point (Fig. 8a). As a comparison, the anatase TiO_2 powders have a lower activation energy (56 ± 3 kJ/mol) (Fig. 8b) for onset coarsening–coalescence given the Arrhenius plot of the $t_{0.5}$ data points 8 ± 2, 4 ± 0.9, 3 ± 0.5, and 1 ± 0.1 min in the linear region of the rate curves, at 700, 800, 900 and 1000 °C, respectively (Fig. 7). As for γ-Al_2O_3 particles 50 and 10 nm in size, the apparent activation energy for the similar event was estimated as 241 ± 18 and 119 ± 19 kJ/mol, respectively indicating easier surface diffusion and particle movement for the latter.[12] A surprisingly low apparent activation energy (77 ± 2 kJ/mol) for the coarsening–coalescence of ZrO_2 nanoparticles in comparison with that of less refractory and small-sized γ-Al_2O_3 before transformation into stable α-Al_2O_3 [12] can be attributed to extensive t → m transformation for enhanced plasticity. In this connection, transformation induced plasticity was experimentally proved for a number of materials.[26] Alternatively oxygen vacancies may facilitate surface diffusion of ZrO_2 at temperatures in air in view of sintering of nanocrystalline zirconia at 550 °C in vacuum or 600 °C in air by surface diffusion.[27] The anatase → rutile transformation did not occur within $t_{0.5}$, i.e. for 50% surface area reduction, in the temperature range of 700–1000 °C for the present TiO_2 nanoparticles. Thus, the onset coarsening–coalescence kinetics based on $t_{0.5}$ in this temperature range has nothing to do with polymorphic transformation. Further sintering of larger-sized TiO_2 in anatase or rutile structure was reported to have a much higher activation energy of

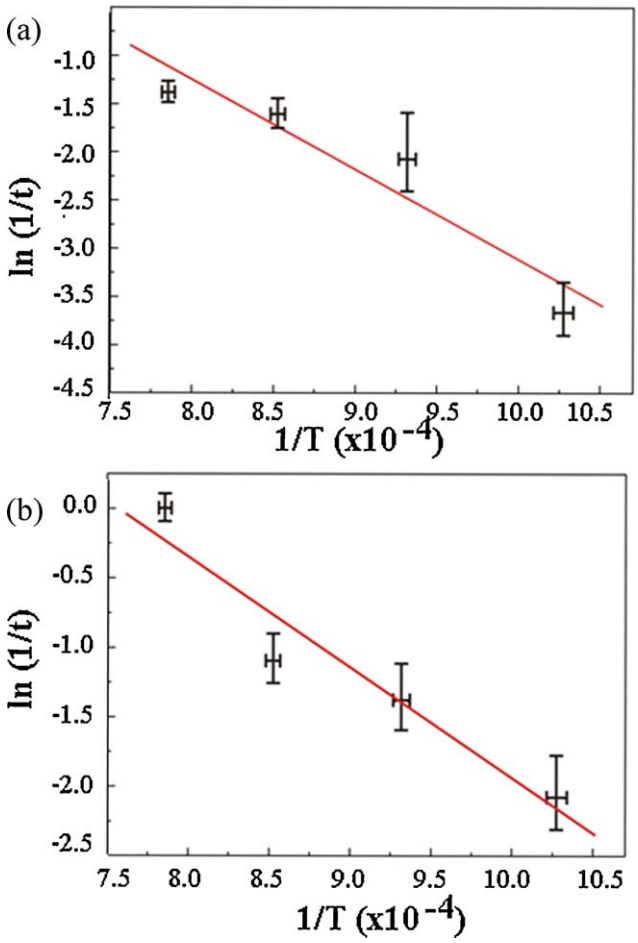

Fig. 8. Arrhenius plots of the logarithmic reciprocal time ($t_{0.5}$ in min) against reciprocal temperature (in Kelvin) for the formation of cylindrical pores and specific surface area decrease by 50% from the dry pressed: (a) ZrO_2 and (b) TiO_2, respectively.

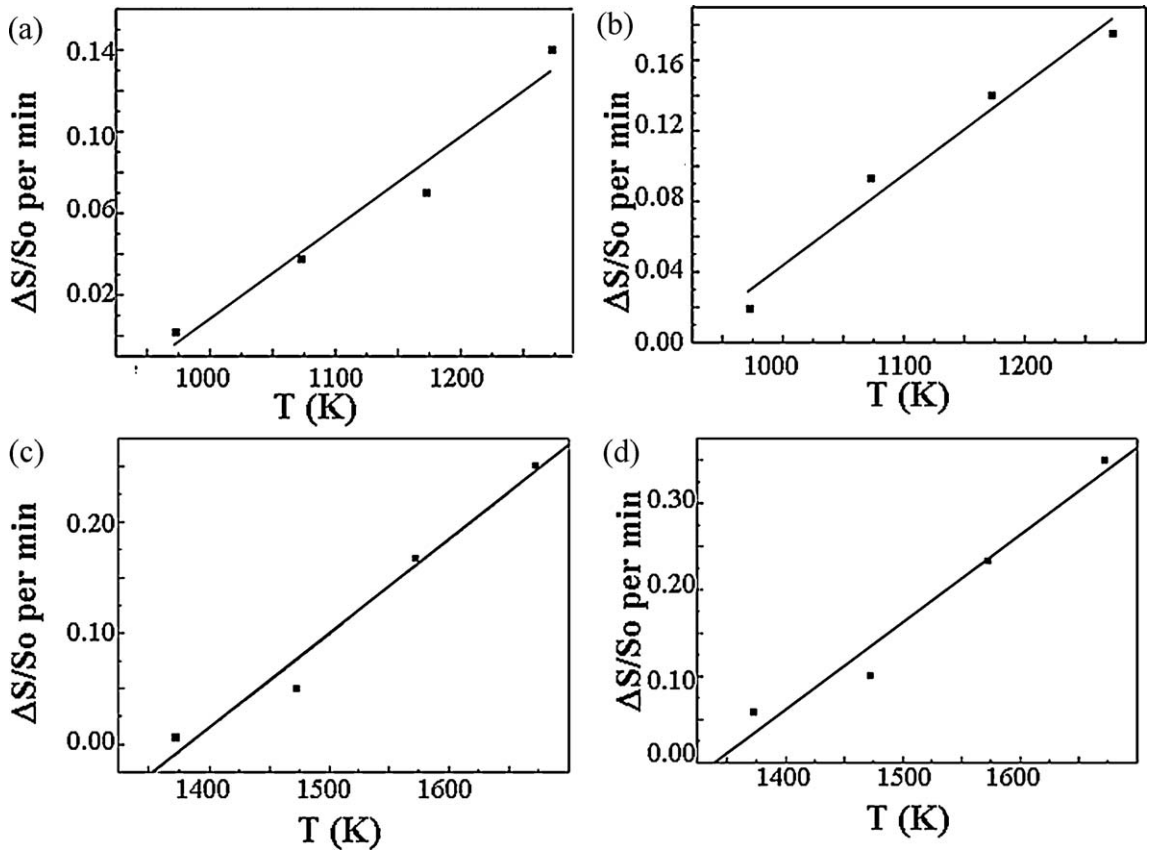

Fig. 9. Temperature dependent specific surface area reduction rate of (a) ZrO_2, (b) TiO_2, (c) and (d) Al_2O_3 nanoparticles of 50 nm and 10 nm average diameter, respectively based on the data of Ref. 12.

284.9 and 259 kJ/mol, for surface- and grain boundary-diffusion controlled process, respectively.[28]

4.3. Effect of specific surface area on phase change

The change of specific surface area in a slightly sintered body is of concern to the polymorphic transformation of ZrO_2 and TiO_2 at high temperatures in air. The t → m transformation of undoped ZrO_2 is expected to occur below 1200 °C at ambient pressure according to the phase diagram.[23] The specific surface area reduction down to 20 m^2/g (Table 1) seems to trigger extensive t → m transformation of the present ZrO_2 nanoparticles slightly sintered at temperatures. Such a surface area dependence of t → m transformation is roughly in accord with the reported size-dependent structural stability of nano-sized ZrO_2 particles.[7,29]

As for the TiO_2 powders, the anatase → rutile transformation, as expected above 600 °C at ambient pressure according to the phase diagram,[30] occurs only when the specific surface area is between 4 and 20 m^2/g, e.g. beyond 5 min at 1000 °C (Table 2). In this connection, thermodynamic calculations suggested that at standard pressure, anatase is more stable than rutile when their particle sizes are below ~14.5 nm.[6,7] This theoretical critical size does not necessarily correspond to the critical specific surface area of anatase → rutile transformation in the present TiO_2 powders with an additional effect of matrix constraint when slightly sintered. In fact, anatase → rutile transformation is facilitated by enhanced ionic mobility at temperatures near the melting point of the nanoparticles according to multiparticle multiphase molecular dynamics (MD) simulations of TiO_2 nanoparticles undergoing sintering-induced phase transformations.[31]

4.4. Minimum temperature of vigorous coarsening–coalescence of nanoparticles in a static or dynamic process

The minimum temperature for vigorous coarsening–coalescence (T_{cr}) of nanoparticles is of concern to the preparation and heterogeneous catalysis use of ZrO_2 and TiO_2 in thin film[9,10] or bulk assembly upon thermal exposure in a static or dynamic process. The T_{cr} is also of mechanical property concern to TZP and TiO_2 polycrystals in view of the improved ductility of sintered polycrystals with particle size reduction.[4]

On the basis of the extrapolation of steady specific surface area reduction rates, i.e. that measured at $t_{0.5}$, to null (Fig. 9), T_{cr} are estimated as 710 and 641 °C, respectively for the present 30–50 nm sized ZrO_2 and 20–50 nm sized TiO_2 nanoparticles, whereas 1111 and 1064 °C, respectively for previously studied 50 nm and 10 nm-sized γ-Al_2O_3 particles.[12] This indicates that such sized ZrO_2 and TiO_2 nanoparticles are able to coarsen and coalesce at temperatures significantly lower than previously thought, i.e. near 1000 °C, for Brownian motion/coalescence of

ZrO_2 and TiO_2[18–21] as well as Al_2O_3[32] nanocondensates into a close packed manner under radiant heating in a dynamic PLA process.

As for nanoparticles finer than 10 nm in size, it is difficult to reliably measure the sintering or coarsening–coalescence rate in static or dynamic heating process for T_{cr} estimation. Still, MD simulation was alternatively used to study the sintering to full coalescence of two small TiO_2 nanoparticles (3 or 4 nm in size)[33] by tracking the shrinkage of the center-to-center distance and the growth of the sintering neck. Their simulations indicated that the process of sintering is strongly affected by temperature (573–1473 K) and initial orientation, and the dipole–dipole interaction between sintering nanoparticles plays a very important role at temperatures away from the melting point thus shedding light on the flame reactors.[33] Further MD study indicated that the acceleration achieved by the graphical processing units, originally developed for the visualization of highly realistic computer games, allowed simulating two TiO_2 nanoparticles (<5 nm) sintering from adhesion and neck growth to finally full coalescence over several hundred nanoseconds via surface diffusion at 1800 K.[34]

5. Conclusions

1. BET/BJH adsorption–desorption hysteresis isotherms of nanosized t-ZrO_2 and anatase TiO_2 powders were used satisfactorily to determine the time for the steady change of specific surface area as a characteristic of an onset coarsening–coalescence event.
2. In the temperature range of 700–1000 °C, the powder underwent onset sintering coupled with coarsening–coalescence before polymorphic transformation of TiO_2, but accompanied with t → m transformation of ZrO_2. The critical specific surface area is 20 m^2/g for t → m transformation of ZrO_2 and 4–20 m^2/g for anatase → rutile transformation of TiO_2.
3. The apparent activation energy for onset sintering–coarsening–coalescence of for ZrO_2 and TiO_2 nanoparticles was estimated as 77 ± 2 and 56 ± 3 kJ/mol. Surprising low apparent activation energy for the ZrO_2 nanoparticles in comparison with that for less refractory and small-sized γ-Al_2O_3 nanoparticles can be attributed to extensive t → m transformation of ZrO_2 for enhanced plasticity.
4. The minimum temperature for coarsening–coalescence of the ZrO_2 and TiO_2 nanoparticles are 710 and 641 °C based on the extrapolation of steady specific surface area reduction rates to null. This critical temperature is significantly lower than previously thought, i.e. near 1000 °C, for the two nanocondensates under radiant heating in a dynamic PLA process.

Acknowledgments

We thank Drs. C.N. Huang and S.Y. Chen for helpful discussion on the coalescence of nanoparticles in a dynamic laser ablation condensation process. Supported by Center for Nanoscience and Nanotechnology at NSYSU and National Science Council, Taiwan, ROC.

Appendix 1.

XRD (CuKα) traces of the ZrO_2 powders: (a) dry-pressed, (b), (c) and (d) further fired at 800 °C for 8 min, 900 °C for 6 min and 1000 °C for 5 min, respectively having strong diffractions of the m-symmetry and strong to weak diffractions of the t-symmetry as labeled.

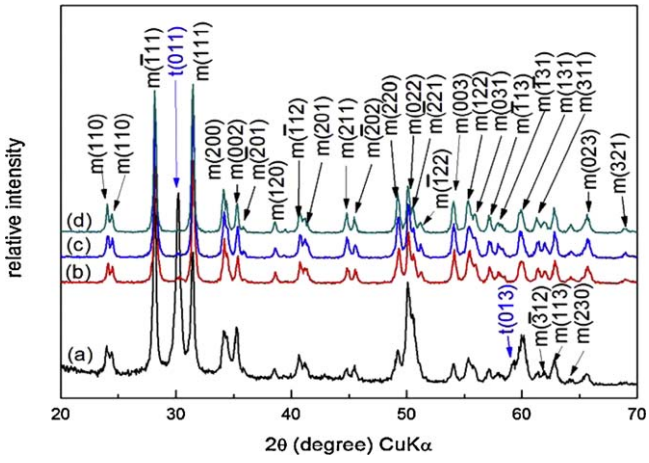

Appendix 2.

XRD (CuKα) traces of the TiO_2 powders subjected to various treatments: (from bottom to top) dry-pressing, further fired at 900 °C for 5 min, 1000 °C for 5 min, 1000 °C for 7 min, and 1000 °C for 10 min, respectively having strong to moderate strong diffractions of the polymorphs labeled. The diffractions indexing of anatase and rutile (only for samples fired at 1000 °C for more than 7 min), are after JCPDS files 21-1272 and 21-1276, respectively.

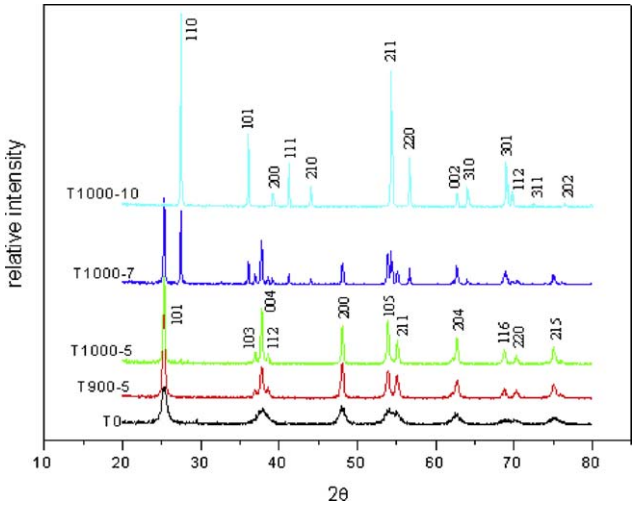

References

1. Häfele E, Kaltenmaier K, Schönauer U. Application of the ZrO_2 sensor in determination of pollutant gases. *Sensors Actuators B: Chem* 1991;**4**:525–7.
2. Garvie RC. The occurrence of metastable tetragonal zirconia as a crystallite size effect. *J Phys Chem* 1965;**69**:1239–43.
3. Green DJ, Hannink RHJ, Swain MV. *Transformation toughening of ceramics*. CRC Press Inc.; 1989. p. 1–232.
4. Karch J, Birringer R, Gleiter H. Ceramics ductile at low temperature. *Nature* 1987;**330**:556–8.
5. Schiavello M. *Photocatalysis and environment*. Dordrecht: Kluwer Academic Publishers; 1988.
6. Zhang H, Banfield JF. Thermodynamic analysis of phase stability of nanocrystalline titania. *J Mater Chem* 1998;**8**:2073–6.
7. Banfield JF, Zhang H. Nanoparticles in the environment. *"Nanoparticles and the environment," reviews in mineralogy and geochemistry*, vol. 44; 2001. Chapter 1, p. 1–58.
8. Bond GC. *Heterogeneous catalysis principles and applications*. Oxford: Oxford University Press; 1992. p. 1–176.
9. Chen IM, Yeh SW, Chiou SY, Gan D, Shen P. Condensation of tetragonal zirconia polycrystals by reactive sputtering. *Thin Solid Films* 2005;**491**:339–46.
10. Kao CH, Yeh SW, Huang HL, Gan D, Shen P. A study of the TiO to anatase transformation by thermal oxidation of Ti film in air. *J Phys Chem C* 2011;**115**:5648–56.
11. Goldstein AN, Echer CM, Alivisatos AP. Melting in semiconductor nanocrystals. *Science* 1992;**256**:1425–7.
12. Liu IL, Shen P. Onset coarsening/coalescence kinetics of γ-type related Al_2O_3 nanoparticles: implications to their assembly in a laser ablation process. *J Eur Ceram Soc* 2009;**29**:2235–48.
13. Yeh Y, Liu IH, Shen P. Onset coarsening/coalescence of cobalt oxides in the form of nanoplates vs. equi-axed micron particles. *J Eur Ceram Soc* 2010;**30**:677–88.
14. Liu IH, Shen P. Coarsening, coalescence and sintering of hexagonal ZnO elongated nanoparticles. *Ceram Int* 2010;**36**:1289–96.
15. Brunauer S, Emmett PH, Teller E. Adsorption of gases in multimolecular layers. *J Am Chem Soc* 1938;**60**:309–19.
16. Barrett EP, Joyner LG, Halenda PP. The determination of pore volume and area distribution in porous substances. I. Computations from nitrogen isotherms. *J Am Chem Soc* 1951;**73**:373–80.
17. Jang HD, Friedlander SK. Restructuring of chain aggregates of titania nanoparticles in the gas phase. *Aerosol Sci Technol* 1998;**29**: 81–91.
18. Tsai MH, Chen SY, Shen P. Imperfect oriented attachment: accretion and defect generation of nanosize rutile condensates. *Nano Lett* 2004;**4**:1197–201.
19. Tsai MH, Chen SY, Shen P. Condensation and relaxation/transformation of dense t-ZrO_2 nanoparticles. *J Chem Phys* 2005;**122**:2047081–6.
20. Tsai MH, Shen P, Chen SY. Defects generation of anatase nanocondensates via coalescence and transformation from dense fluorite-type TiO_2. *J Appl Phys* 2006;**100**:114313-1–6.
21. Tsai MH, Chen SY, Shen JP, Shen P. Laser ablation condensation of polymorphic ZrO_2 nanoparticles: effects of laser parameters, residual stress and kinetic phase change. *J Appl Phys* 2006;**99**:054302-1–8.
22. Sing KSW, Everett DH, Haul RAW, Moscou L, Pierotti RA, Rouquerol J, et al. Reporting physisorption data for gas/solid systems with special reference to the determination of surface area and porosity. *Pure Appl Chem* 1985;**57**:603–19.
23. Whitney ED. Electrical resistivity and diffusionless phase transformations of zirconia at high temperatures and pressures. *J Electrochem Soc* 1965;**112**:91–4.
24. Chen PL, Chen IW. Sintering of fine oxide powders. *J Am Ceram Soc* 1997;**80**:637–45.
25. Deer WA, Howie RA, Zussman J. *An introduction to the rock-forming minerals*. 2nd ed. Longman Scientific and Technical; 1992 p. 548–553.
26. Poirier JP. *Creep of crystals – high-temperature deformation processes in metals, ceramics and minerals*. Cambridge: Cambridge Univ. Press; 1985.
27. Śŕdic VV, Winterer M, Hahn H. Sintering behavior of nanocrystalline zirconia prepared by chemical vapor synthesis. *J Am Ceram Soc* 2000;**83**:729–36.
28. Seto T, Shimada M, Okuyama K. Evaluation of sintering of nanometer-sized titania using aerosol method. *Aerosol Sci Technol* 1995;**23**:183–200.
29. Zhang YL, Jin XJ, Rong YH, Hsu TY, Jiang DY, Shi JL. The size dependence of structural stability in nano-sized ZrO_2 particles. *Mater Sci Eng A* 2006;**438–440**:399–402.
30. Dachille F, Simons PY, Roy R. Pressure–temperature studies of anatase, brookite, rutile, and TiO_2 (II). *Am Mineral* 1968;**53**:1929–39.
31. Koparde VN, Cummings PT. Phase transformations during sintering of titania nanoparticles. *ACS Nano* 2008;**2**:1620–4.
32. Pan C, Chen SY, Shen P. Laser ablation condensation, coalescence and phase change of dense γ-Al_2O_3 particles. *J Phys Chem B* 2006;**110**:24340–5.
33. Koparde VN, Cummings PT. Molecular dynamics simulation of titanium dioxide nanoparticle sintering. *J Phys Chem B* 2005;**109**:24280–7.
34. Buesser B, Gröhn AJ, Pratsinis SE. Sintering rate and mechanism of TiO_2 nanoparticles by molecular dynamics. In: *2011 AIChE annual meeting*. 2011.